remote sensing

Article

Detection of Macroalgal Bloom from Sentinel−1 Imagery

Sree Juwel Kumar Chowdhury [1,2], Ahmed Harun-Al-Rashid [3], Chan-Su Yang [1,2,4,*] and Dae-Woon Shin [1,2]

1 Maritime Security and Safety Research Center, Korea Institute of Ocean Science & Technology, Busan 49111, Republic of Korea; jusau65@kiost.ac.kr (S.J.K.C.); sin6535@kiost.ac.kr (D.-W.S.)
2 Department of Convergence Study on the Ocean Science and Technology, Ocean Science and Technology School, Korea Maritime & Ocean University, Busan 49112, Republic of Korea
3 Department of Aquatic Resource Management, Sylhet Agricultural University, Sylhet 3100, Bangladesh; rashidmha.arm@sau.ac.bd
4 Marine Technology and Convergence Engineering, University of Science & Technology, Daejeon 34113, Republic of Korea
* Correspondence: yangcs@kiost.ac.kr

Abstract: The macroalgal bloom (MAB) is caused by brown algae forming a floating mat. Most of its parts stay below the water surface, unlike green algae; thus, its backscatter value becomes weaker in the synthetic aperture radar (SAR) images, such as Sentinel−1, due to the dampening effect. Thus, brown algae patches appear to be thin strands in contrast to green algae and their detection by using a global threshold, which is challenging due to a similarity between the MAB patch and the ship's sidelobe in the case of pixel value. Therefore, a novel approach is proposed to detect the MAB from the Sentinel−1 image by eliminating the ship's sidelobe. An individually optimized threshold is applied to extract the MAB and the ships with sidelobes from the image. Then, parameters are adjusted based on the object's area information and the ratio of length and width to filter out ships with sidelobes and clutter objects. With this method, an average detection accuracy of 82.2% is achieved by comparing it with the reference data. The proposed approach is simple and effective for detecting the thin MAB patch from the SAR image.

Keywords: macroalgal bloom; brown algae; SAR; Sentinel−1

check for updates

Citation: Chowdhury, S.J.K.; Harun-Al-Rashid, A.; Yang, C.-S.; Shin, D.-W. Detection of Macroalgal Bloom from Sentinel−1 Imagery. *Remote Sens.* **2023**, *15*, 4764. https://doi.org/10.3390/rs15194764

Academic Editor: Chung-Ru Ho

Received: 17 August 2023
Revised: 20 September 2023
Accepted: 25 September 2023
Published: 28 September 2023

1. Introduction

The macroalgal bloom (MAB) refers to the growth of any type of macroalgae, which typically takes place in eutrophic waterbodies such as bays, coastal waters, etc. [1]. It has been reported that frequent massive MAB events occurred in waterbodies around the world during the past three decades [2]. Sometimes, the excessive MAB leads to serious marine environmental issues as well as huge economic loss when it becomes deposited on beaches. For example, more than $2.91 million per year is consumed for cleaning up the deposited macroalgae on the beaches of Texas [3].

Despite being a global concern, a small−scale MAB event occurred in 2007 in the Yellow Sea (YS) [4]. However, in the next year a huge amount of the MAB (*Ulva prolifera*) suddenly deposited close to the Olympic Sports Center in Qingdao coastal areas of the YS, China, and thus received mass public attention [5]. Afterwards, it became a common phenomenon during mid−May and until July in that region [6–8]. Moreover, a huge amount of seaweed (brown seaweed *Sargassum*) mats piled up along the southwest islands of the Korean Peninsula and Jeju Island's coasts in the northern part of the East China Sea (ECS) [9]. Previously, the presence of *Sargassum* was reported only in the oceanic front between the Kuroshio Current and continental shelf of the ECS [10], but unexpected distribution was detected in 2012 after the accumulation of brown algae rafts along the northern coast of Taiwan [10,11]. In the ECS, the MAB area caused by the brown algae is seen from March to May [12]. From an ocean research station such as Ieodo Ocean Research Station (IORS), located in the southwest of the Korean Peninsula (Figure 1), it is occasionally feasible to observe the macroalgae patches. IORS was built to acquire significant information on the local air and sea environments of the ECS so that a thorough understanding of their influence on Korea's marine and atmospheric environments could be attained. Recently, a bi−macroalgal bloom has occurred in the YS through the co−occurrence of green and brown algae [10]. This indicates the increasing degree of the MAB expansion over the YS and the ECS with time.

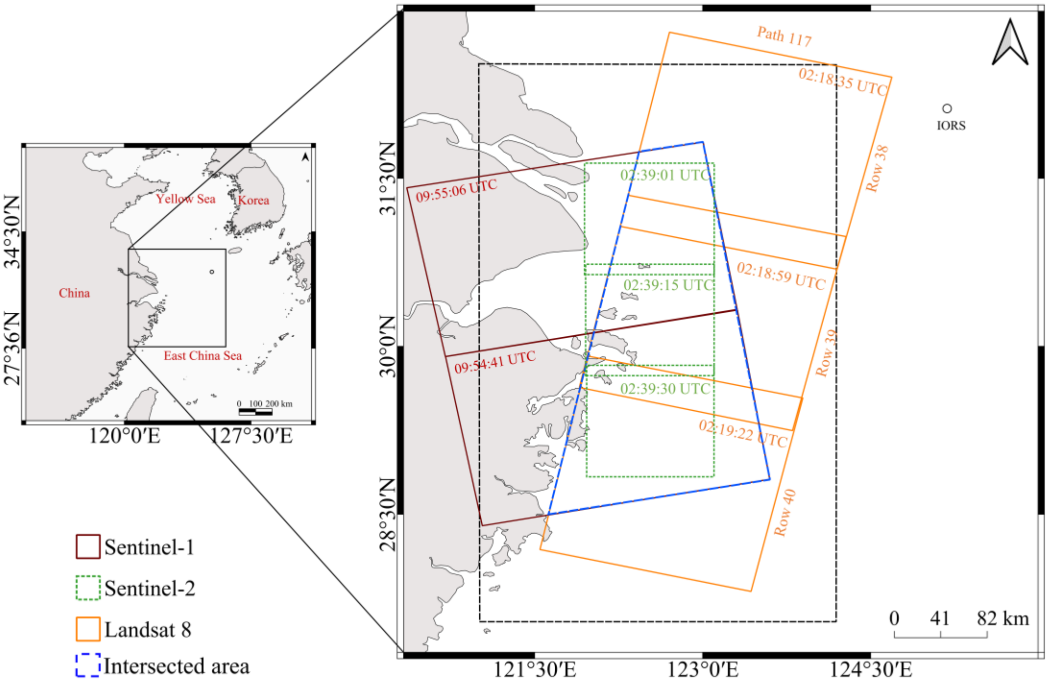

Figure 1. Location of the studied region shows the boundaries of Sentinel−1 (brown rectangles), Sentinel−2 (green dashed rectangles), and Landsat 8 (yellow rectangles) images. The blue−colored box indicates the intersection area of Landsat 8 and Sentinel−1 images. The black−dashed rectangle indicates the area used for visualizing the sea surface wind and surface current circumstances. Black circle indicates the location of Ieodo Ocean Research Station (IORS).

For accurate detection of the MAB distribution, satellite−based remote sensing provides an effective way for detecting the spatiotemporal variation in the blooms and furthers the understanding of the possible cause of their occurrences [13]. Most of the earlier research works on the MAB have been conducted by utilizing images by different optical satellite sensors such as the medium resolution imaging spectrometer, the moderate resolution imaging spectroradiometer, and the Geostationary Ocean Color Imager, etc. [9,14,15]. However, those satellites have moderate resolution, cloud obstruction, and lack of night observation which could be overcome by utilizing synthetic aperture radar (SAR) images to detect the MAB [16,17]. A previous study [18] demonstrated the capacity of the SAR data to distinguish between various ocean surface features including ocean currents, slicks, and winds by using co−polarized (VV and HH) images for polarization differences, polarization ratios, and nonpolarized components. The SAR data also have the potential to detect the MAB by utilizing the backscattering radar waves, which are called the normalized radar cross section (NRCS) [19]. Generally, macroalgae remain floating on the water surface and act as solid features, generating significant volume scattering against the emitted radar pulses [19,20]. Consequently, the MAB produces brighter pixels than the surrounding seawater pixels, and most often appears as irregular slicks, belts, or dots and thus provides a theoretical basis for extracting the MAB areas [17,19]. The detection is greatly dependent on the distinction between the MAB's NRCS and other feature signals, such as ships, lands, and other ocean phenomena, including currents and ocean fronts, as the backscatter signal of the MAB is comparatively weaker than the mentioned features [16]. Previous works on the MAB were based on the SAR images that mainly focused on the detection of the green tides which produce large floating mats and have more ability to stay above the water surface most of the time compared to the those of brown macroalgae, with their appearance in the SAR image being visually distinguishable from other features [16,19–21]. Shen et al. [16] developed a new index for the RADARSAT−2 quad−polarized SAR images to extract the green tide from the seawater based on the unsupervised method. Gao et al. [20] developed a deep learning model, AlgaeNet model, for detecting the green tide caused by *Ulva prolifera* from the moderate resolution imaging spectroradiometer and the SAR images. Guo et al. [19] proposed a texturally enhanced deep learning model on the basis of the classic U−net framework to detect the green tide from the Sentinel−1 image. Ma et al. [17] combined optical the moderate resolution imaging spectroradiometer and Sentinel−1 images to investigate the spatiotemporal distribution of the green tide that occurred in the YS. Contrary to this, a smaller number of studies using the SAR images have been conducted in the case of the MAB detection caused by *Sargassum*. *Sargassum* bloom generates floating mats on the water surface which mostly remain below the water surface [8]. It also generates longer thin patch formations during shifts [22] where the individual patch sizes vary from 10 to 300 cm in length [8]. On the contrary, the length of a single green macroalgae patch varies from 18 to 100 cm [8]. In the case of microwave remote sensing, the surface backscattering signal returns from the MAB parts which stay at the water surface, whereas no signal comes from the submerged part of the MAB which results in a weak appearance of the MAB in the SAR images. Therefore, due to this morphological characteristic, the detection of the macroalgae from the SAR imagery is difficult in contrast to the optical images. Additionally, stronger radar returns occur in co−polarized (VV) images in comparison with the cross−polarized (VH) images [16]. However, the detection of these thin−shaped MABs from co−polarized images is challenging as the ship's sidelobe interferes in the detection process due to possessing a similar backscatter value. On the other hand, in cross−polarized images, no sidelobe appears with the ship; however, the appearance of the MABs is comparatively less than in the co−polarized images.

Therefore, the purpose of this study was to propose a method for detecting the bloom caused by the macroalgae from the dual−polarized Sentinel−1 SAR images by eliminating the ship's sidelobe. Subsequently, the results of the Sentinel−1 MAB detection approach were presented by displaying the spatial distribution map. Moreover, the Landsat 8 and Sentinel−2 images, considered as the additional data almost concurrent to Sentinel−1, were used to display the spatial distribution and temporal changes of the MABs within the Sentinel−1 coverage region for a short−time period.

2. Materials and Methods

2.1. Study Area and Data

The studied area ranged from 121°E to 124°E and 28°N to 32°N (Figure 1), covering both the YS and the ECS where the MABs frequently appear from March to May. The YS is a shallow partially closed continental shelf that is connected to the Bohai Sea (from the northwest) and the ECS (from the south). It is situated in the Western Pacific Ocean between the Chinese Mainland and the Korean Peninsula.

In this research work, the SAR data from Sentinel−1 and optical images from both the Landsat 8 and Sentinel−2 satellites were used. The Sentinel−1 image was used for detecting even the small patches of macroalgae, whereas Landsat 8 and Sentinel−2 images were utilized to display the spatial distribution of the MAB within the Sentinel−1 covered area (Figure 1). Sentinel−1 comprises two polar orbiting satellites denoted as Sentinel−1A and Sentinel−1B, each of which are outfitted with a C−band synthetic aperture radar equipment and are operated at a 5.405 GHz central frequency; therefore, imagery can be captured at both day and night without being affected by the weather. Sentinel−1 Level−1 Ground Range Detected (GRD) products, which were generated from the Single Look Complex data utilizing multi−looking and ground range projection employing an earth ellipsoid model, were used in this study. Sentinel−1 dual-polarized GRD data (Table 1) covering the studied site was procured from the Copernicus Open Access Hub website (https://scihub.copernicus.eu/; accessed on 20 March 2022). Moreover, Sentinel−2 Level 1C images were used in this study, which provided 13 spectral bands with different spatial resolutions. Level 1C products were atmospherically corrected (top−of−atmosphere), and the selected Sentinel−2 images (Table 1) were obtained from the Copernicus Open Access Hub website. The Landsat 8 satellites carry two instruments, the Operational Land Imager and the Thermal Infrared Sensor; therefore, they provided both spectral and thermal surface images of the planet [13]. The images consisted of a total of 11 bands that included visible, NIR, shortwave infrared (SWIR), and thermal infrared (TIR) bands. The selected Landsat 8 Level 1 Collection 1 data (Table 1) were downloaded from the United States Geological Survey website (https://earthexplorer.usgs.gov/; accessed on 20 March 2022). In this study, Sentinel−1 images captured on 7 April 2021 were employed to fabricate the MAB detection steps while Sentinel−1 images captured on 19 April 2021 were used to verify the MAB detection approach.

Table 1. Satellite data used for this study.

Satellite	Product	Polarization/Total Bands	Path and Row	Acquisition Time (UTC)		Resolution
				Date	Center Time	
Sentinel−1	Level 1 GRD	VV + VH	-	7 April 2021	09:55:06	10 m
					09:54:41	
				19 April 2021	09:55:06	
					09:54:41	
Landsat 8	Collection 1 Level 1	11	117, 38	6 April 2021	02:18:35	30 m
			117, 39		02:18:59	
			117, 40		02:19:22	
Sentinel−2	Level 1C	13	T51RVQ	20 April 2021	02:39:01	10 m
			T51RVP		02:39:15	
			T51RVN		02:39:30	

The sea surface wind and surface current data were used to understand the circumstances of wind and current during the MAB detection period. Therefore, global coverage of hourly instantaneous sea surface wind and hourly mean surface current model data were procured from the Copernicus Marine Service website (https://marine.copernicus.eu/; accessed on 25 May 2022). The spatial resolutions of the wind and current model data used in this study were $0.125° \times 0.125°$ [23] and $0.083° \times 0.083°$ [24], respectively. The distribution of sea surface wind and surface current in the studied region during the MAB detection time was depicted by using these model data.

2.2. Methodology

2.2.1. Data Preprocessing

The Sentinel Application Platform (SNAP; ver. 8.0) was used for Sentinel−1 data preprocessing [25]. The preprocessing phase comprised orbit correction, thermal noise removal, radiometric calibration, speckle filtering (Lee Sigma), range Doppler terrain correction, and decibelization of radar backscatter coefficients in sequence, which were performed by batch processing in the SNAP [25,26].

The Landsat 8 images were used in this study for illustrating the spatial distribution of the MAB within the Sentinel−1 coverage area (Figure 1). To process the Landsat 8 image, the Atmospheric Correction for Operational Land Imager "lite" software (ACOLITE; ver. 20170718.0) [13,27] was used which aids in simple and fast data processing. By using this software, the Rayleigh scattering corrections were performed with the help of a 6SV−based lookup table, illumination, and viewing geometry information such as the zenith of sun and sensor, and the angles of azimuth [28,29].

In this study, geometrically and radiometrically corrected L1C Sentinel−2 images were utilized to visualize the spatial distribution of bloom area across the Sentinel−1 coverage [30].

2.2.2. Postprocessing

The Sentinel−1 image contains two polarization channels defined as co−polarized (VV) and cross−polarized (VH) images. The co−polarized image displays enhanced returns of radar signal over open sea areas compared to the cross−polarized image, and this occurs due to Bragg scattering in co−polarization and volume scattering in cross−polarization [16]. Ocean processes can generate gravity waves on the water surface, which makes the surface rough and returns a strong signal, whereas these generations have no apparent impact on volume scattering [16] and therefore macroalgae become more visible in a co−polarized image (Figure 2a). Thus, the Sentinel−1 co−polarized VV (dB) image was selected for the MAB detection work. Additionally, the connectivity of the MAB patch in the co−polarized image was more obvious than in the cross−polarized image, where the part of the same MAB patch appeared to be distinct.

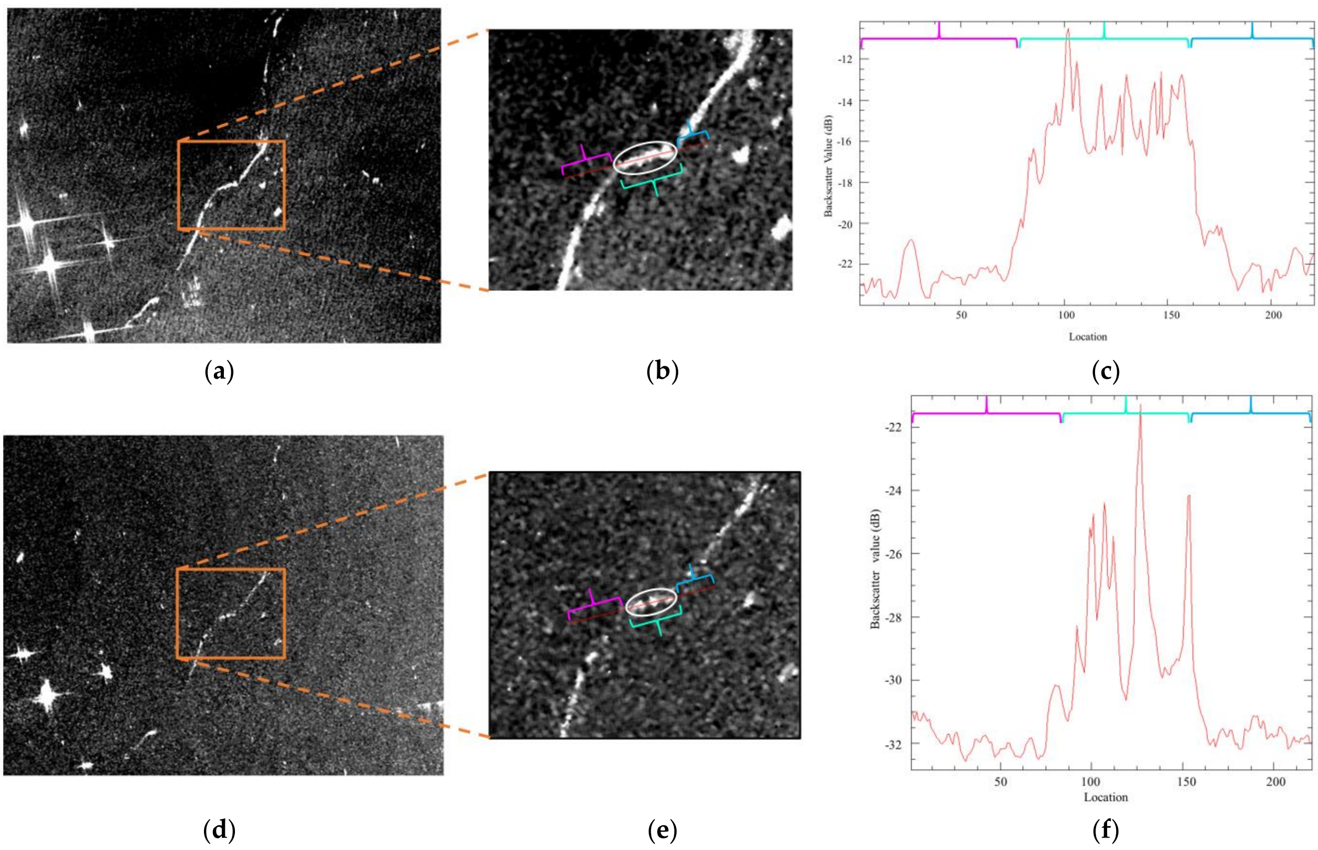

Figure 2. Macroalgae patches in (**a**) co−polarized VV (dB), and (**d**) cross−polarized VH (dB) images. Cross sections (red line) in images (**b**,**e**) represent the backscatter value (dB) of pixels in images (**c**,**f**). White circle = macroalgae patch, pink and blue color = water pixels, and cyan color = macroalgae pixels.

Although Sentinel−1 images are generally less contaminated by clouds and illumination, the detection method of macroalgae from Sentinel−1 depended on the capability of creating a difference between the macroalgae backscatter signal and other features (such as ships, islands, and ocean processes) of the signals [16]. Moreover, bloom coverage areas caused by brown algae were less visible in the SAR image due to their submerged condition. Therefore, firstly, visual interpretation was performed on the Sentinel−1 images to find out the area where the MAB−like features (shape such as strands, belt, or dots) appeared. During this process, areas with the MAB−like features were figured out, and then those areas were clipped very roughly from the two Sentinel−1 images by excluding the land part. The total number of clipped areas was 12, and these areas were denoted as the regions of interests (ROIs). Each of these ROIs contains all features, including ships, macroalgae, and other interferences (clutter) present in the whole image (Figure 3).

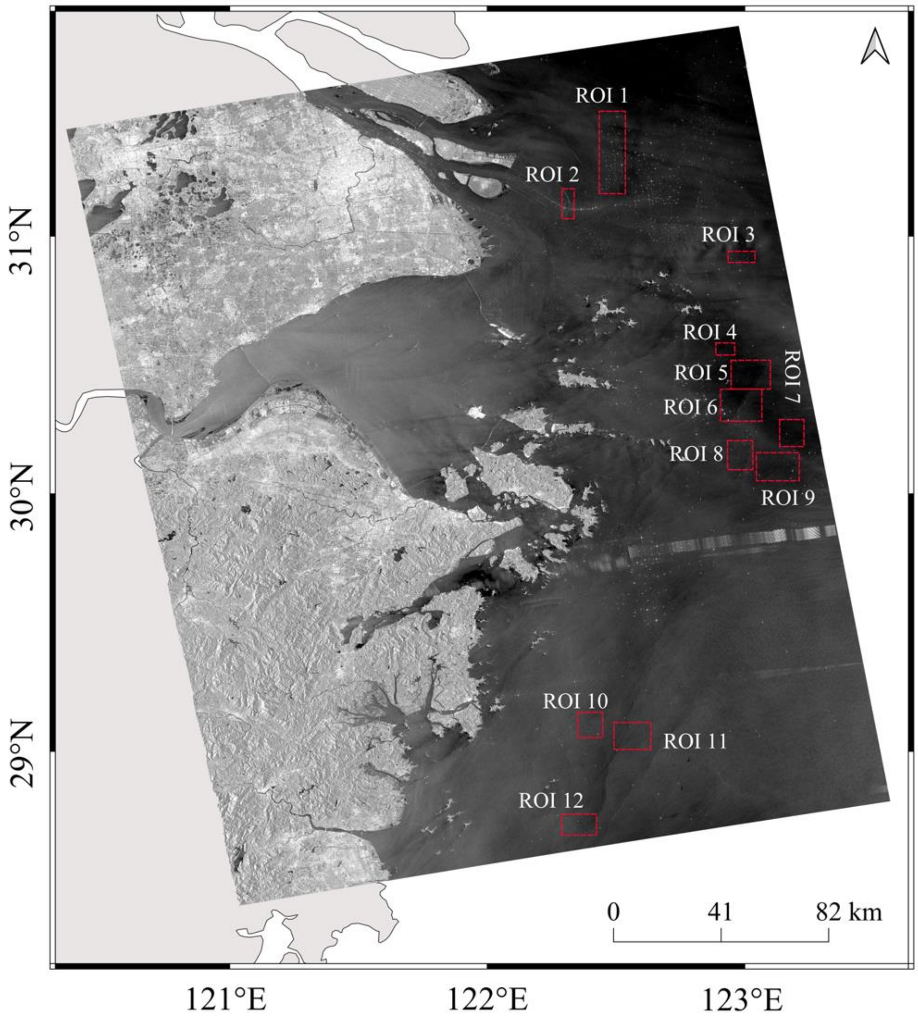

Figure 3. Boundary of 12 ROI areas in the mosaic of two Sentinel−1 VV (dB) images acquired on 7 April 2021. Dashed red rectangles indicate the ROI areas.

An approach based on the object extraction was conducted to extract the target object, the MAB, by removing all non−target features on the basis of the object size and aspect ratio. The flowchart representing the steps conducted for each ROI is schematized in Figure 4. In the first step, an individually optimized threshold value was applied to the ROI image to extract the target objects (bright pixels) from the dark background (sea water pixels). Through the thresholding operation, bright pixels were separated from the dark background and generated objects of different sizes, which represent the features present in the image. The threshold values were different for each ROI area as the value range of the MAB features varied with the background condition. The threshold value for each ROI was selected based on trial−and−error analysis (Table 2). Furthermore, these threshold values were applied to the Sentinel-1 images acquired on 19 April 2021, and, on the basis of trial−and−error analysis, threshold values were selected for the detection of bloom areas.

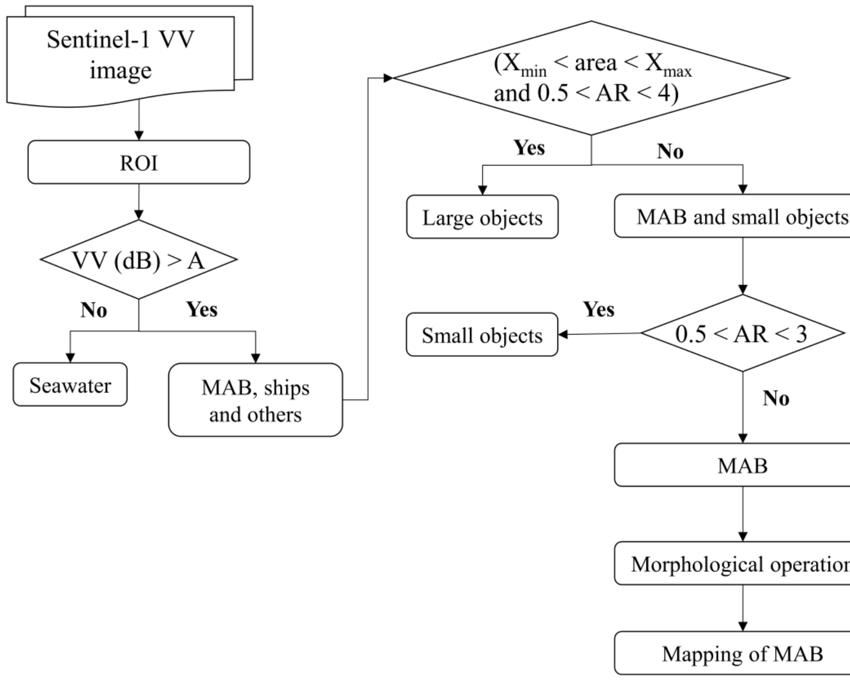

Figure 4. Schematic flowchart of the proposed MAB detection approach. 'A' indicates the individually optimized threshold value. AR = aspect ratio of object, X_{min} = minimum area of object, X_{max} = maximum area of object.

Table 2. The threshold values of each ROI.

ROI No.	1	2	3	4	5	6	7	8	9	10	11	12
Threshold value (dB)	−18	−17	−19	−20	−20	−18	−20	−19	−19	−17	−17	−16

A binary image was created through thresholding which includes the MAB, ships, and some clutter areas. Among these binarized objects, non−target objects (ship and clutter features) were filtered out in two steps. Generally, objects belonging to ships occupy a larger area than the objects generated from clutter pixels and the aspect ratio, which measures the object's footprint in a ratio of length to width [31] and is also different in comparison with the clutter object. Moreover, some features belonging to ships and macroalgae can be occupied by the same size. However, the aspect ratio of ships and macroalgae is different as ships appear as a cross−like structure in VV (dB) polarization (due to the ship's sidelobe). Therefore, they both have a long width and length compared to the MAB, which forms a long strand. As a result, by utilizing the aspect ratio, objects that were generated from the ship feature can be separated from the target object (MAB) and thus, based on the size and aspect ratio, large and small objects were filtered out of the binarized image.

Based on this condition, both large and small objects were filtered out separately. In the case of filtering large objects (ships), the aspect ratio ranged from 0.5 (1:2) to 4 (4:1), and in relation to filter small objects (clutter), the aspect ratio from 0.5 (1:2) to 3 (3:1), were both maintained. The object size varied from image to image; therefore, the range of the object area was determined by trial−and−error analysis based on each ROI image. To remove the large objects, the adopted minimum object sizes (X_{min}) from ROI 1 to ROI 12 were 0.009, 0.0004, 0.12, 0.01, 0.05, 0.06, 0.04, 0.08, 0.07, 0.07, 0.07, and 0.049 km^2, respectively, whereas the maximum object sizes (X_{max}) from ROI 1 to ROI 12 were 0.6, 0.7, 0.2, 0.013, 0.15, 0.8, 0.2, 0.4, 0.2, 0.3, 0.12, and 0.15 km^2, respectively. Afterwards, morphological operations, including opening and closing, were performed by using a 3 $\times$ 3 structuring elements to eliminate the remaining undefined objects. The illustration of this proposed method is depicted in Figure 5.

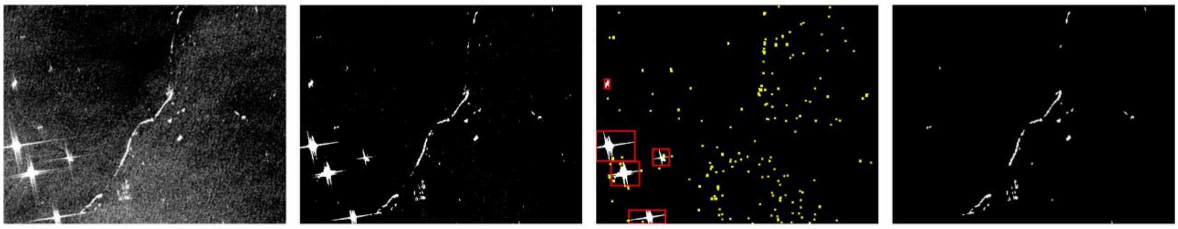

(a) (b) (c) (d)

Figure 5. Illustration of different steps of the proposed method. (**a**) ROI from the Sentinel−1 VV (dB) image. (**b**) Result after thresholding. (**c**) Detecting large objects (red boxes) and small objects (yellow boxes) for removal. (**d**) Final MAB detection result.

A reference dataset was manually created from the same Sentinel−1 images to assess the accuracy of the MAB detection results. To create the reference dataset, a threshold value (−20 dB) was applied in the Sentinel−1 images for the extraction of the MAB pixels; additionally, the extraction findings included other features (ship, land−coast area, speckle noise, etc.). Then, the extraction result was imported into QGIS and transformed into vectors for further modification. Afterwards, the non−target objects, such as ships, parts of land, and other interferences, were eliminated manually to obtain the MAB features. After obtaining the MAB detection result from Sentinel−1 image by utilizing the proposed approach (Figure 5), a comparison between the detected MAB area and the manually extracted MAB area from Sentinel−1 was conducted. The detection accuracy was assessed in terms of percentage area (Figure 3) of detection matched with the reference dataset.

In the case of the Landsat 8 image, the postprocessing part consisted of the calculation of the Floating Algae Index (FAI) that was obtained from the R_{rc} images. In contrast to the baseline subtraction technique, FAI was calculated and highlighted the red-edge reflectance of flora for the MAB detection [27,31].

$$\text{FAI} = R_{rc,\text{NIR}} - [R_{rc,\text{Red}} + (R_{rc,\text{SWIR}} - R_{rc,\text{Red}}) \times \{(\lambda_{\text{NIR}} - \lambda_{\text{Red}})/(\lambda_{\text{SWIR}} - \lambda_{\text{Red}})\}], \quad (1)$$

where Red, NIR, and SWIR are Landsat 8 bands at 655, 865, and 1609 nm of spectral reflectance, respectively, and the wavelength of these bands is represented by the symbol λ.

After deriving the FAI image, the next step was to detect the MAB area. To accomplish this, the areas covered by the macroalgae were masked out with care to include whole macroalgae patches. During this process, care was taken to exclude ships, clouds, and lands from the masked area. As macroalgae can be detected under thin clouds from FAI−derived images, cloud masking was not applied directly [27,32]. After masking the MAB covered area, a generalized minimum threshold value of 0 was used for the FAI to eliminate the water pixels and to assume that the remaining pixels belong to the MAB area. The MAB detection result obtained from the Landsat 8 images was then used to display the distribution of the bloom area within the intersect region (Figure 1).

Additionally, the MAB detection results from Sentinel−1 and Landsat 8 were compared, a macroalgae patch that was visually matched based on its length and shape was identified, and the shift of the matched patch was measured by calculating its centroid displacement, which occurred by 31 h. The shift distance of the macroalgae patch was estimated based on the standard haversine distance formula, which measures the distance among two locations on the sphere [14,33].

Furthermore, for detecting the MAB in Sentinel−2 images, the Normalized Difference Vegetation Index (NDVI) was calculated, which is commonly used to monitor the ocean vegetation [14]. NDVI images were derived by utilizing the following equation [14]:

$$\text{NDVI} = (R_{\text{NIR}} - R_{\text{Red}})/(R_{\text{NIR}} + R_{\text{Red}}) \quad (2)$$

where R_{NIR} and R_{Red} represent the reflectance of NIR (865 nm) and red (655 nm) bands, respectively. The NDVI value ranges between −1 and +1.

Afterwards, the MAB was extracted from the NDVI calculated images by employing the same procedure performed with the Landsat 8 FAI images. A generalized minimum threshold value of 0.18 was adopted to extract the MAB by excluding the water pixels because the positive NDVI value indicated vegetation [14]. Then, the detection results from Sentinel−2 images were mapped to display the spatial distribution of the bloom area within the Sentinel−1 covered region (Figure 1). Similar to FAI, NDVI is also used for detecting the MAB; thus, FAI and NDVI were used for Landsat 8 and Sentinel−2, respectively, to depict the spatial distribution of the MAB. In addition, despite the absence of field data, the MAB detection result from Landsat 8 and Sentinel−2 images, which covered the same area as the Sentinel−1 images (intersected area, Figure 1), indirectly validated the Sentinel−1 MAB detection result (presence of macroalgae patches around Landsat 8 and Sentinel−2 detection result), as the scene capture time of the Landsat 8 and Sentinel−2 was closest to the Sentinel−1 image acquisition time.

3. Results

3.1. Detection of Macroalgal Bloom from Sentinel−1

In the case of the Sentinel−1 images on 7 April 2021, the proposed detection method was applied to 12 roughly generated ROI areas, and detection results by using this method are depicted in Figure 6. The MAB in ROI areas, the reference data for related ROI areas, and the binary MAB detection results of this proposed method are shown in Figure 6a–c. In comparison to the manually extracted MAB, the average detection accuracy of the MAB with this proposed approach was 82.2%. From Figure 6c, it can be seen that features related to ships as well as the clutter features were completely removed. Afterwards, due to the morphological operation, the remaining clutter features were also eliminated, and only the object representing the macroalgae was present in the final binary image.

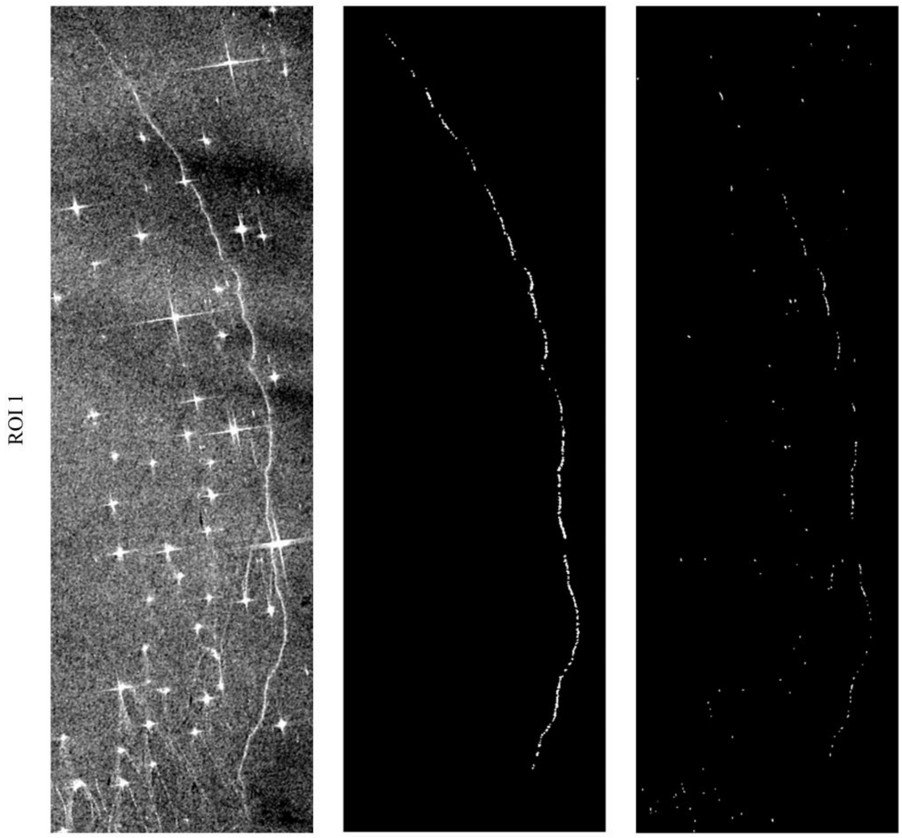

Figure 6. *Cont.*

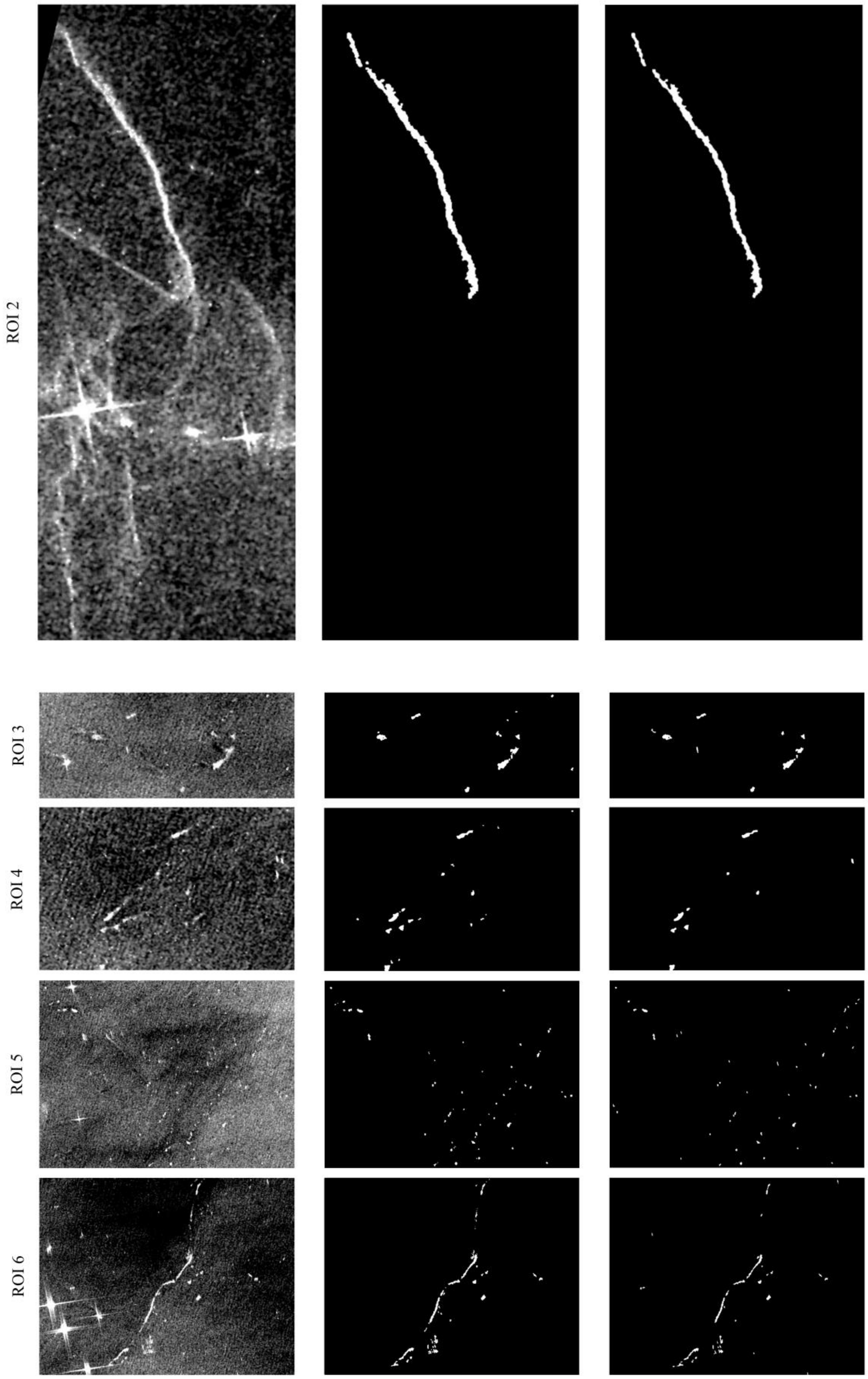

Figure 6. *Cont.*

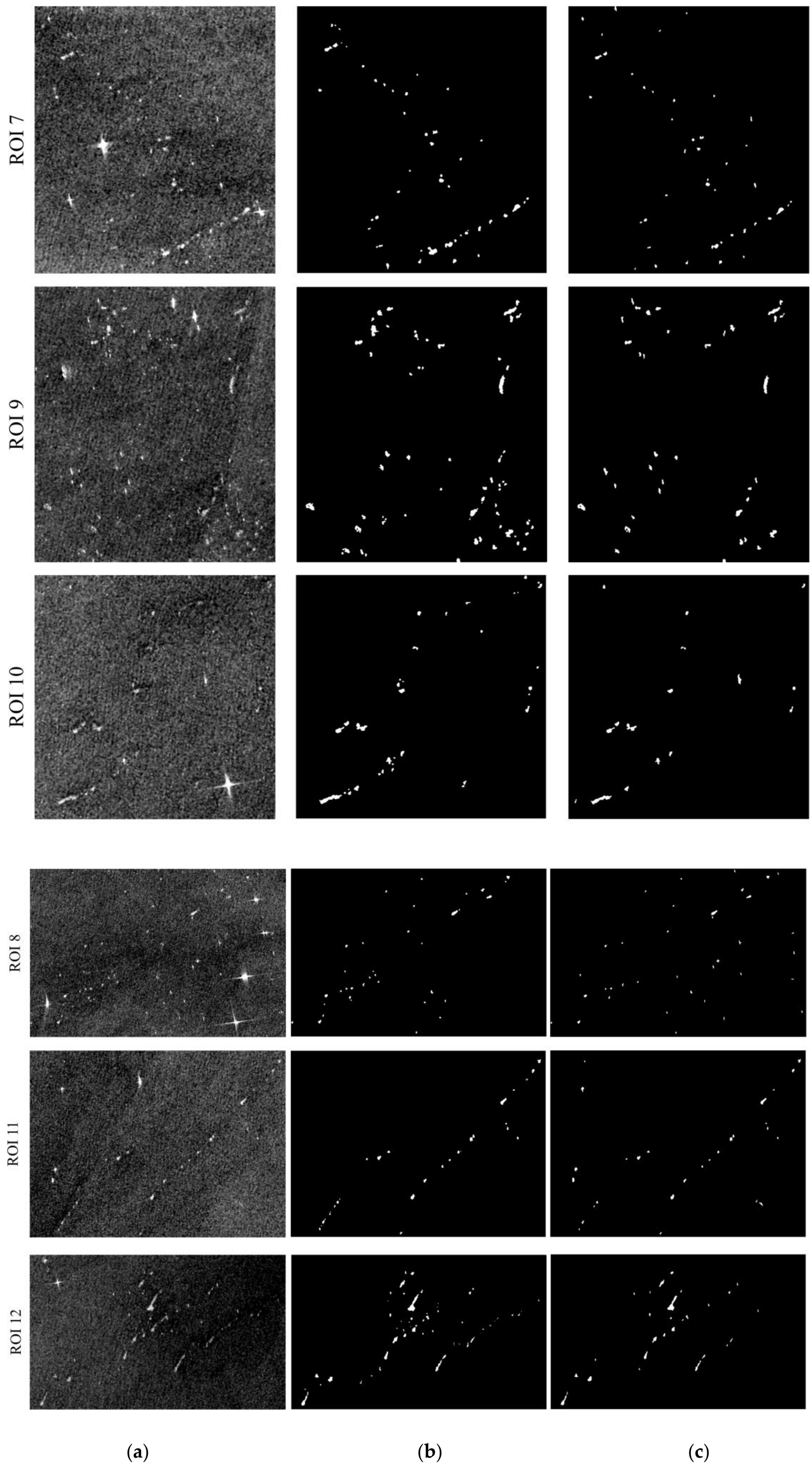

Figure 6. Macroalgal bloom detection results for different ROI areas. (**a**) Sentinel−1 VV (dB) image. (**b**) Reference data. (**c**) The proposed method.

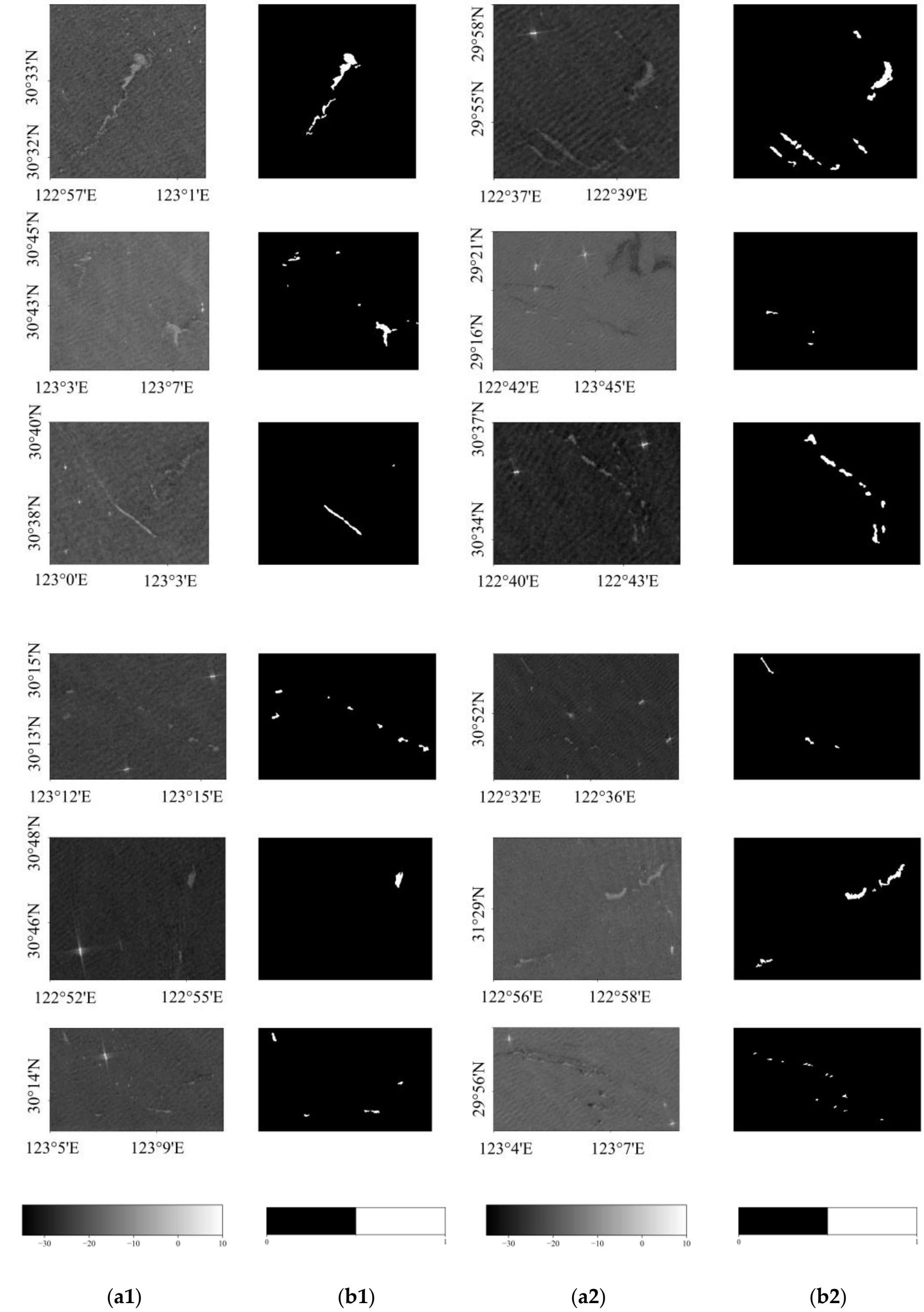

Figure 7. Examples of macroalgal bloom detection result from the Sentinel−1 (19 April 2021) images. (**a1,a2**) Sentinel−1 VV (dB) image. (**b1,b2**) Detection results were obtained using the proposed approach.

The highest performance of this method was found in ROI 2 and the accuracy was 98.1%. The detection accuracy for ROI 1, ROI 3, ROI 4, ROI 5, ROI 6, ROI 7, ROI 8, ROI 9, ROI 10, ROI 11, and ROI 12 were 62.2%, 89.2%, 79.9%, 83.5%, 91.3%, 78.8%, 81.3%, 67.2%, 75.9%, 93.9%, and 84.8%, respectively.

To verify the proposed approach, two other Sentinel−1 images performed within a different period (19 April 2021) were used. Some examples of the detection result are depicted in Figure 7, which show that by utilizing the proposed approach, the ships and other interferences were removed and only the MAB area remained.

The threshold values employed in this detection (−18, −19, and −20) remained within the range of values that were previously determined (Table 2).

3.2. Temporal Changes of Macroalgal Bloom Patches Using Sentinel−1, Landsat 8, and Sentinel−2 for a Short−Term Period (31 h)

After the detection of macroalgae from the Sentinel−1 and Landsat 8 images, mapping was performed to visualize the distribution of bloom areas. Figure 8 depicts the map of the MAB distribution in the YS and the ECS on 6 and 7 April 2021. Figure 8 shows that the MAB dispersion region was adjacent to the coast of China. Moreover, the MAB detected from Sentinel−1 images occupied approximately 6.8 km^2, whereas the coverage of the MAB detection from Landsat 8 was approximately 62.1 km^2.

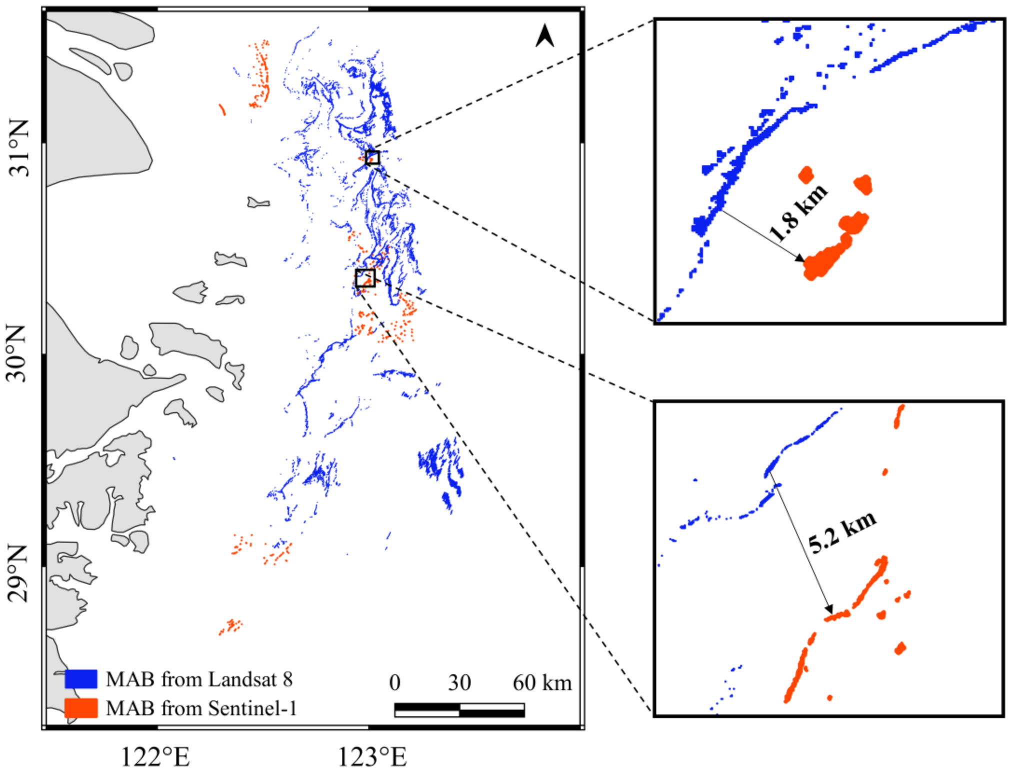

Figure 8. Distribution of macroalgal bloom area detected from Sentinel−1 (7 April 2021; 02:19 UTC) and Landsat 8 (6 April 2021; 02:19 UTC) within the intersected area (Figure 1). The black rectangles show the shift of the macroalgae patch. The arrow within the black rectangle indicates the shift direction (from the previous location to the present location) of macroalgae. In the case of the Sentinel−1 detection result, the pixel size is exaggerated for increased visuality.

Additionally, the speed and direction of the sea surface wind and surface current on the corresponding days, which correlated with the satellite images, were also mapped to understand the situation and shift of macroalgae patches. Figure 9 represents the wind and current distribution maps for two days. The wind flowed in a southwest direction on 6 April 2021, and the direction was maintained for the next day as well. The wind speed on 6 April and 7 April 2021 was mild and ranged from 3 m/s to 5 m/s (29°N to 31.5°N, 122°E to 123.5°E) within the macroalgae detected region. Therefore, it can be assumed that the macroalgae patches maintained their shape (strands, belts, or dots) for these two days as the wind speed was not very strong. Moreover, the surface current speed was also not strong on those days and remained between 0.1 m/s and 0.2 m/s (29°N to 31.5°N, 122°E to 123.5°E); however, the direction of the surface current was different on both days. On 6 April, the direction was northeastward at middle latitude (29°N to 30.5°N) and westward at higher latitude; on 7 April 2021, the direction of the surface current was northeastward. Thus, these results allow hypothesize that a long−distance shift of macroalgae patches did not occur.

To calculate the shift of the macroalgae patches, it was important to identify the same patches. In this case, two patches were visually matched after comparing the Sentinel−1 and Landsat 8 MAB detection results, which are shown in Figure 8. The time difference between the macroalgae detection times from two satellites was approximately 31 h. During this time, a shift of the MAB happened. From the detection result of the MAB from Sentinel−1 (Figure 6c), it can be seen that the part of the macroalgae patch was detected separately due to its submerged condition in water. With this limitation, it was difficult to find a macroalgae patch that visually matched the patch detected from the Landsat 8 image. Figure 8 also depicts the shift direction as well as the shift distance of the macroalgae patches between the detection times. Macroalgae patches shifted in the southeastward direction, and the shift distances were 1.8 and 5.2 km, respectively. Moreover, it was found that the shift speed of macroalgae patch was approximately 0.2 km/h (0.06 m/s).

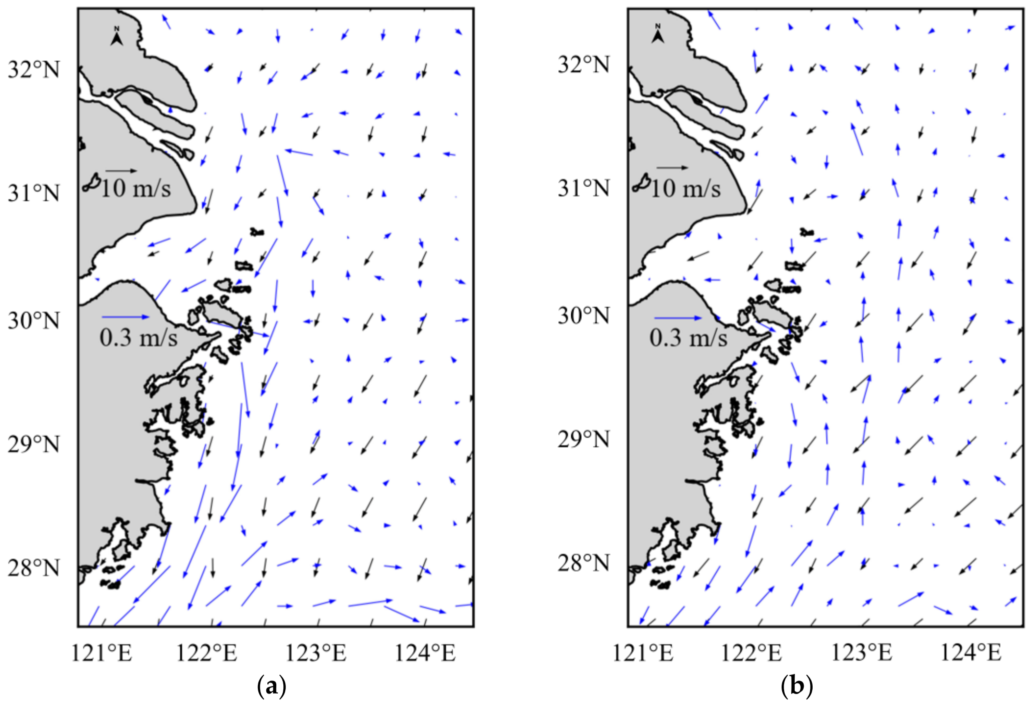

Figure 9. Distribution of ocean surface wind and surface current. Black and blue arrows indicate the direction of wind and current, respectively (direction they were flowing to). (**a**) Wind: 6 April 2021 02:00 UTC. Current: 6 April 2021 02:30 UTC. (**b**) Wind: 7 April 2021 10:00 UTC. Current: 7 April 2021 09:30 UTC.

Additionally, the outcomes of the MAB detection from the Sentinel−1 and Sentinel−2 images from a different time period (19 and 20 April 2021) are depicted in Figure 10. The MAB coverage area was found to be approximately 6.8 km^2 and 21.97 km^2 for Sentinel−1 and Sentinel−2, respectively. The MAB dispersion region was the same as the prior period (Figure 10).

Figure 11 also shows the surface wind and current conditions during that time. It was discovered that the wind speed was substantially higher (8 m/s) on 19 April 2021 compared to 7 April 2021, and that it was blowing in a westward direction. In addition, compared to the prior MAB detection time, the surface current speed was also higher (0.4 m/s).

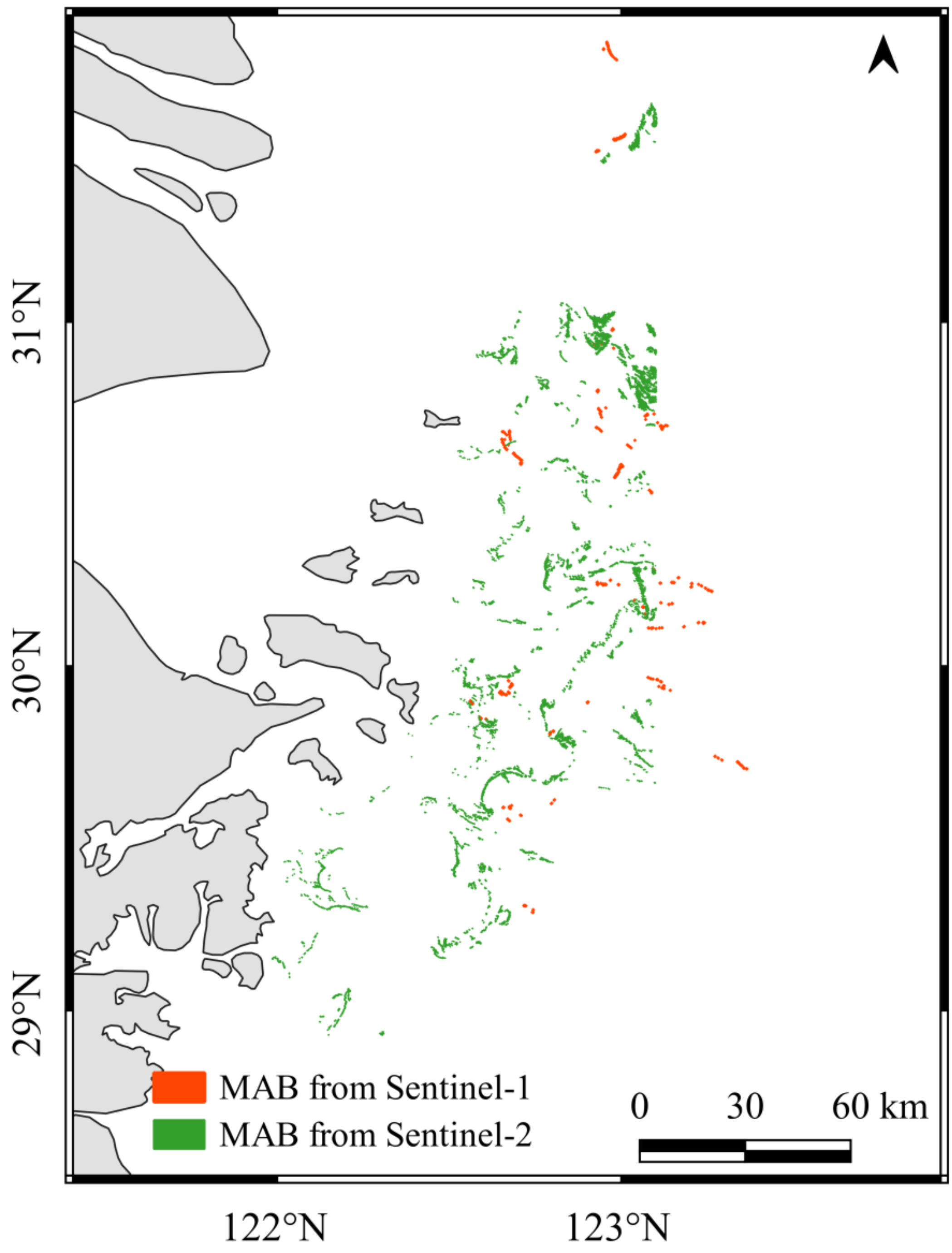

Figure 10. Distribution of macroalgal bloom area detected from Sentinel−1 (19 April 2021; 09:55 UTC) and Sentinel−2 (20 April 2021; 02:39 UTC) within the intersecting area (Figure 1). The pixel size is exaggerated for better visuality.

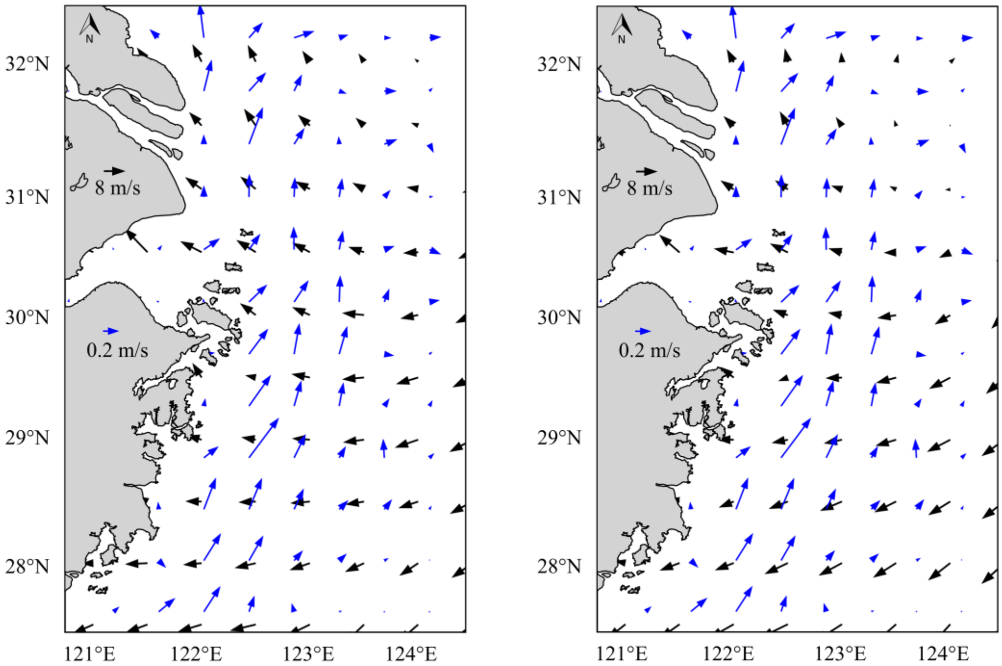

(**a**) (**b**)

Figure 11. Distribution of ocean surface wind and current. Black and blue arrows indicate the direction of wind and current, respectively. (**a**) Wind: 19 April 2021 10:00 UTC. Current: 19 April 2021 09:30 UTC. (**b**) Wind: 20 April 2021 03:00 UTC. Current: 20 April 2021 02.30 UTC.

4. Discussion

In this study, bloom caused by the *Sargassum* (April is considered as the blooming period of *Sargassum*) was detected from the Sentinel−1 SAR and optical Landsat 8 and Sentinel−2 images (Figures 8 and 10). Previous MAB detection works using the SAR data were mainly focused on the detection of *Ulva*, which is denoted as green algae. However, bi−microalgal bloom due to the cooccurrence of green and brown algae over the YS and the ECS depicts the high expansion intensity of macroalgal bloom. Therefore, the detection of the brown algae from the SAR image is important for detection and monitoring to continue with the optical image and even when the optical image becomes unavailable or obstructed by the cloud cover. According to prior works on the *Sargassum* detection using the SAR data, it has been found that the MAB features appeared much smaller and formed a thinner shape in the SAR image than the corresponding optical image in the same area [8]. Therefore, automatic detection of that bloom area using the SAR image is challenging compared to the optical image. The key motivation of this work was to develop a method to detect the thin−shaped MAB from the Sentinel−1 image. Figures 6 and 7 display the results of the proposed MAB detection method.

Selecting both target and non−target objects and then filtering only non−target objects based on the object extraction approach is the basic concept of this method. By applying this concept, ships and most of the clutter features were selected after the thresholding operation based on their size and aspect ratio was performed. Afterwards, these non−target features were eliminated to only obtain the target features that belong to the macroalgae. In the case of ROI 2, the MAB detection accuracy was 98.1%, and, on the contrary, ROI 1 showed the lowest accuracy (62.2%), which happened due to the presence of a high number of clutter pixels and by separately detecting the MAB in that image. This situation occurred because some parts of the same macroalgae patch remained below the water surface while some parts stayed at the water surface; thus, an irregular appearance within the same macroalgae patch occurred in the Sentinel−1 image. Although most of the clutter features were removed during the filtering operation, some of them could not be eliminated due to their similarity with the individual macroalgae clumps in terms of size and aspect ratio. Additionally, the MAB detection results and accuracy (82%), in the case of Sentinel−1 images that were acquired on 19 April 2021 (Figure 7), were equivalently consistent with the prior findings (Figure 6), suggesting that the proposed approach has the ability to extract the MAB in different situations.

Figure 8 illustrates the distribution of bloom over the YS and the ECS detected from the Sentinel−1 and Landsat 8 images, in which the scene capture time difference between the Sentinel−1 and Landsat 8 was around 31 h. In Landsat 8 images, the detected bloom coverage was higher (62.1 km^2) than the coverage (6.8 km^2) in Sentinel−1 images. Similar findings are displayed in Figure 10, where the Sentinel−2's MAB detected area was larger (21.97 km^2) than Sentinel−1's (6.8 km^2) and the scene capture time disparity was the same. Theoretically, the detection of macroalgae in the SAR image depends on two mechanisms [8]. The first mechanism is that floating macroalgae rafts can suppress the ocean surface waves, and, due to the smooth surface, weak backscattering occurs and leads to the appearance of macroalgae to have a negative contrast (dark color), such as other marine slicks in the SAR [8]. Second, as an aquatic plant, macroalgae possess leaves, stems, and air sacs that generally spread over the water surface during the bloom period; thus, they act as a strong reflector and produce a positive contrast (bright color) in the SAR image [8]. In the case of our study, the MAB produced a positive contrast (Figure 7a) in the Sentinel−1 images. However, although having an air sac, *Sargassum* remained just beneath the surface of the water most of the time; thus, their detection from Sentinel−1 became impossible as no bloom feature appeared in that image. This happened due to the strong water absorption characteristics of the C−band radar signal; therefore, most of the bloom did not appear. On the contrary, optical bands can penetrate into the water to some extent. As a result, for the MAB that stay 1 cm beneath the water surface, 95% of the optical signal can be reflected to the sensor [8]. Thus, less MAB was detected from the Sentinel−1 images in comparison to the Landsat 8 and Sentinel−2 images. Additionally, Figures 9 and 11 represent the distribution of ocean surface wind and surface current on 6, 7, 19, and 20 April, respectively. It was found that wind and current had less impact on the detection of macroalgae from Sentinel−1 as the speed of both wind (<5 m/s) and current (<0.2 m/s) was mild in the case of the MAB detection area on 7 April 2021. While the wind and current conditions were different on 19 April 2021, both the wind and current speed were higher than the prior period. However, the MAB detection area was the same in both periods. Therefore, an assumption can be made that the detection performance of macroalgae from Sentinel−1 images depends on the capability of brown algae to stay above the water surface.

Figure 8 depicts the MAB distribution detected from the Sentinel−1 and Landsat 8 images over the studied region. After comparing the detection results from the Sentinel−1 and Landsat 8 images, two macroalgae patches were identified that were visually matched. More patches were identified from the detection result as the macroalgae patches were not matched visually. There was a 31 h gap between the detection results from the two satellites; within this time, a shift of macroalgae occurred. Moreover, the MAB that remained in the submerged condition were not detected in the Sentinel−1 image; in some cases, parts of a large macroalgae patch were detected separately. Therefore, the same patch could not be visualized in its entirety from the Sentinel−1 detection result.

The proposed method was applied and conducted in a different period (19 April 2021), and it showed a promising result in the case of the thin MAB patch detection from the Sentinel−1 SAR data. Although the criteria used in this approach, such as threshold value, object area, and aspect ratio, are not consistent and will be changed with the selected image, an improvement approach can be taken by adopting more precise detection criteria or making those criteria consistent. Moreover, further research can be conducted by applying this approach in a different polarization channel to obtain a more enhanced detection result. Furthermore, this method can be applied in other SAR image with different wavelength (X−band, L−band) to detect the MAB. Additionally, the submerged parts of the MAB do not appear in the Sentinel−1 SAR image, and therefore only the MAB part that remained at the water surface can be detected from the other SAR image as well. Moreover, the MABs are more visible in the co−polarized image than the cross-polarized image, and the concurrent use of other co−polarized channels such as HH with VV polarization that possess 10 m or less than 10 m resolution can aid in detecting the MAB more precisely. Thus, the detection result from the proposed approach can be improved by using different polarization images from the other SAR bands with high resolution.

5. Conclusions

In this study, emphasis was placed on detecting a thin MAB patch of *Sargassum* from the Sentinel−1 image by combining the threshold and object extraction methods. With the comparison of manually extracted detection results, an average of 82% of detection accuracy was achieved using this approach. Additionally, the net shift distance and shift speed of the macroalgae patches were measured after comparing the detection result from the optical Landsat 8 image. This method is simple and efficient in comparison to the manual selection and deletion process after binarization. Thus, this method of MAB detection from a Sentinel−1 SAR image can help in detecting the bloom area—particularly, it helped in identifying the area which formed a thin patch and appeared separately from the large MAB patch—and in monitoring the shift of macroalgae patches when optical images are not available or are encountered by clouds.

Author Contributions: Conceptualization, S.J.K.C., A.H.-A.-R. and C.-S.Y.; methodology, S.J.K.C., A.H.-A.-R., C.-S.Y. and D.-W.S.; software, S.J.K.C. and A.H.-A.-R.; validation, A.H.-A.-R. and C.-S.Y.; formal analysis, S.J.K.C., A.H.-A.-R., C.-S.Y. and D.-W.S.; investigation, S.J.K.C., A.H.-A.-R. and C.-S.Y.; resources, S.J.K.C., A.H.-A.-R. and C.-S.Y.; data curation, S.J.K.C., A.H.-A.-R., C.-S.Y., and D.-W.S.; writing—original draft preparation, S.J.K.C.; writing—review and editing, A.H.-A.-R., S.J.K.C. and C.-S.Y.; visualization, S.J.K.C.; A.H.-A.-R. and C.-S.Y.; supervision, C.-S.Y.; project administration, C.-S.Y.; funding acquisition, C.-S.Y. All authors have read and agreed to the published version of the manuscript.

Funding: This research received no external funding.

Data Availability Statement: The Sentinel−1 and Sentinel−2 images used in this study are openly available on the Copernicus Open Access Hub website (https://scihub.copernicus.eu/). Atmospherically corrected Landsat 8 Collection 1 Level 1 data (DN) were downloaded from the United States Geological Survey website (https://earthexplorer.usgs.gov/), which are not available in this website after December, 2022. However, Landsat 8 Collection 2 Level 1 data (DN) can be used, which is available on the United States Geological Survey website (https://earthexplorer.usgs.gov/). Ocean surface and current data are openly available on the Copernicus Marine Service website (https://marine.copernicus.eu/).

Acknowledgments: This research was supported by Korea Institute of Marine Science & Technology Promotion (KIMST) funded by the Ministry of Oceans and Fisheries (20210607, Establishment of the Ocean Research Station in the Jurisdiction Zone and Convergence Research). Parts of this study were conducted using E.U. Copernicus Marine Service Information.

Conflicts of Interest: The authors declare no conflict of interest.

References

1. Yabe, T.; Ishii, Y.; Amano, Y.; Koga, T.; Hayashi, S.; Nohara, S.; Tatsumoto, H. Green tide formed by free-floating *Ulva* spp. at Yatsu tidal flat, Japan. *Limnology* **2009**, *10*, 239–245. [CrossRef]
2. Wang, M.; Hu, C.; Barnes, B.B.; Mitchum, G.; Lapointe, B.; Montoya, J.P. The great Atlantic *Sargassum* belt. *Science* **2019**, *365*, 83–87. [CrossRef] [PubMed]
3. Webster, R.K.; Linton, T. Development and implementation of *Sargassum* early advisory system (SEAS). *Shore Beach* **2013**, *81*, 1–6.
4. Liu, D.; Keesing, J.K.; Xing, Q.; Shi, P. World's largest macroalgal bloom caused by expansion of seaweed aquaculture in China. *Mar. Pollut. Bull.* **2009**, *58*, 888–895. [CrossRef] [PubMed]
5. Lee, J.H.; Pang, I.C.; Moon, I.J.; Ryu, J.H. On physical factors that controlled the massive green tide occurrence along the southern coast of the Shandong Peninsula in 2008: A numerical study using a particle-tracking experiment. *J. Geophys. Res.* **2011**, *116*, C12036. [CrossRef]
6. Xu, Q.; Zhang, H.; Cheng, Y.; Zhang, S.; Zhang, W. Monitoring and tracking the green tide in the Yellow Sea with satellite imagery and trajectory model. *IEEE J. Sel. Top. Appl. Earth Obs. Remote Sens.* **2016**, *9*, 5172–5181. [CrossRef]

7. Choi, D.-L.; Noh, J.-H.; Ryu, J.-H.; Lee, J.-H.; Jang, P.-K.; Lee, T.; Choi, D.-H. Occurrence of green macroalgae (*Ulva prolifera*) blooms in the northern East China Sea in summer 2008. *Ocean Polar Res.* **2010**, *32*, 351–359. [CrossRef]
8. Qi, L.; Wang, M.; Hu, C.; Holt, B. On the capacity of Sentinel-1 synthetic aperture radar in detecting floating macroalgae and other floating matters. *Remote Sens. Environ.* **2022**, *280*, 113188. [CrossRef]
9. Park, Y.-J. An analysis on the distribution of floating seaweed in the East China Sea and southern Yellow Sea in 2015—The case of *Sargassum* observed by the Geostationary Ocean Color Imager. *KMI Int. J. Marit. Aff. Fish.* **2020**, *12*, 21–35. [CrossRef]
10. Yuan, C.; Xiao, J.; Zhang, X.; Fu, M.; Wang, Z. Two drifting paths of *Sargassum* bloom in the Yellow Sea and East China Sea during 2019–2020. *Acta Oceanol. Sin.* **2022**, *41*, 78–87. [CrossRef]
11. Komatsu, T.; Mizuno, S.; Natheer, A.; Kantachumpoo, A.; Tanaka, K.; Morimoto, A.; Hsiao, S.-T.; Rothäusler, E.A.; Shishidou, H.; Aoki, M.; et al. Unusual distribution of floating seaweeds in the East China Sea in the early spring of 2012. *J. Appl. Phycol.* **2014**, *26*, 1169–1179. [CrossRef] [PubMed]
12. Qi, L.; Hu, C.; Wang, M.; Shang, S.; Wilson, C. Floating algae blooms in the East China Sea. *Geophys. Res. Lett.* **2017**, *44*, 501–511. [CrossRef]
13. Sun, D.; Chen, Y.; Wang, S.; Zhang, H.; Qiu, Z.; Mao, Z.; He, Y. Using Landsat 8 OLI data to differentiate Sargassum and *Ulva prolifera* blooms in the South Yellow Sea. *Int. J. Appl. Earth Obs. Geoinf.* **2021**, *98*, 102302. [CrossRef]
14. Rashid, A.H.A.; Yang, C.-S. Hourly variation of green tide in the Yellow Sea during summer 2015 and 2016 using Geostationary Ocean Color Imager data. *Int. J. Remote Sens.* **2018**, *39*, 4402–4415. [CrossRef]
15. Hu, C.; Cannizzaro, J.; Carder, K.L.; Muller-Karger, F.E.; Hardy, R. Remote detection of *Trichodesmium* blooms in optically complex coastal waters: Examples with MODIS full-spectral data. *Remote Sens. Environ.* **2010**, *114*, 2048–2058. [CrossRef]
16. Shen, H.; Lu, R.; Li, D. Remote sensing of the Yellow Sea green tide evolution in 2015. *Mar. Sci.* **2016**, *40*, 134–142. [CrossRef]
17. Ma, Y.; Wong, K.; Tsou, J.Y.; Zhang, Y. Investigating spatial distribution of green-tide in the Yellow Sea in 2021 using combined optical and SAR image. *J. Mar. Sci. Eng.* **2022**, *10*, 127. [CrossRef]
18. Kudryavtsev, V.N.; Chapron, B.; Myasoedov, A.G.; Collard, F.; Johannessen, J.A. On dual co-polarized SAR measurements of the ocean surface. *IEEE Geosci. Remote Sens. Lett.* **2013**, *10*, 761–765. [CrossRef]
19. Guo, Y.; Gao, L.; Li, X. A deep learning model for green algae detection on SAR images. *IEEE Trans. Geosci. Remote Sens.* **2022**, *60*, 1–14. [CrossRef]
20. Gao, L.; Li, X.; Kong, F.; Yu, R.; Guo, Y.; Ren, Y. AlgaeNet: A deep-learning framework to detect floating green algae from optical and SAR imagery. *IEEE J. Sel. Top. Appl. Earth Obs. Remote Sens.* **2022**, *15*, 2782–2796. [CrossRef]
21. Yu, H.; Wang, C.; Li, J.; Sui, Y. Automatic extraction of green tide from GF-3 SAR images based on feature selection and deep learning. *IEEE J. Sel. Top. Appl. Earth Obs. Remote Sens.* **2021**, *14*, 10598–10613. [CrossRef]
22. Shin, J.; Lee, J.-S.; Jang, L.-H.; Lim, J.; Khim, B.-K.; Jo, Y.-H. *Sargassum* detection using machine learning models: A case study with the first 6 months of GOCI-II imagery. *Remote Sens.* **2021**, *13*, 4844. [CrossRef]
23. Copernicus Marine Service. Global Ocean Hourly Sea Surface Wind and Stress from Scatterometer and Model. Available online: https://data.marine.copernicus.eu/product/WIND_GLO_PHY_L4_NRT_012_004/download?dataset=cmems_obs-wind_glo_phy_nrt_l4_0.125deg_PT1H_202207 (accessed on 10 February 2023).
24. Copernicus Marine Service. Global Ocean Physics Analysis and Forecast. Available online: https://data.marine.copernicus.eu/product/GLOBAL_ANALYSISFORECAST_PHY_001_024/download?dataset=cmems_mod_glo_phy_anfc_merged-uv_PT1H-i (accessed on 10 February 2023).
25. Moskolaï, W.R.; Abdou, W.; Dipanda, A.; Kolyang. A workflow for collecting and preprocessing Sentinel-1 images for time series prediction suitable for deep learning algorithms. *Geomatics* **2022**, *2*, 435–456. [CrossRef]
26. Fillipponi, F. Sentinel-1 GRD preprocessing workflow. *Proceedings* **2019**, *18*, 11. [CrossRef]
27. Rashid, A.H.A.; Yang, C.-S. Improved detection of tiny macroalgae patches in Korea bay and Gyeonggi bay by modification of floating algae index. *Remote Sens.* **2018**, *10*, 1478. [CrossRef]
28. van der Zande, D.; Vanhellemont, Q.; De Keukelaere, L.; Knaeps, E.; Ruddick, K. Validation of Landsat-8/OLI for ocean colour applications with AERONET-OC sites in Belgian coastal waters. In Proceedings of the Ocean Optics Conference, Victoria, BC, Canada, 23–28 October 2016.
29. Vermote, E.; Tanre, D.; Deuze, J.; Herman, M.; Morcrette, J.; Kotchenove, S. Second simulation of a satellite signal in the solar spectrum-vector (6SV). *IEEE Trans. Geosci. Remote Sens.* **2006**, *3*, 675–686.
30. European Space Agency. Technical Guides Sentinel-2 MSI Level-1C Algorithms and Products. Available online: https://sentinels.copernicus.eu/web/sentinel/technical-guides/sentinel-2-msi/level-1c-algorithms-products (accessed on 25 July 2023).
31. Qiu, H.; Li, H.; Wu, Q.; Meng, F.; Ngan, K.N.; Shi, H. A2RMNet: Adaptively aspect ratio multi-scale network for object detection in remote sensing images. *Remote Sens.* **2019**, *11*, 1594. [CrossRef]
32. Hu, C. A novel ocean color index to detect floating algae in the global oceans. *Remote Sens. Environ.* **2009**, *113*, 2118–2129. [CrossRef]
33. Palmer, M.C. Calculation of distance traveled by fishing vessels using GPS positional data: A theoretical evaluation of the sources of error. *Fish. Res.* **2008**, *89*, 57–64. [CrossRef]